Food & Function

ROYAL SOCIETY OF CHEMISTRY

PAPER

View Article Online
View Journal | View Issue

Cite this: *Food Funct.*, 2025, **16**, 9227

Mechanistic insights into *S*-allyl cysteine's insulin-mimetic role: glucose uptake, receptor kinase interaction, and sensitivity recovery in skeletal myotubes

Federica Geddo, [a] Susanna Antoniotti,[a] Giulia Querio, [b] Andrea Occhipinti,[c,d] Gianluca Catucci,[a] Gloria Ciniero, [a] Loris Curatolo,[d,e] Gianfranco Gilardi [a] and Maria Pia Gallo *[a]

S-Allyl cysteine (SAC), the most abundant sulfur-containing compound present in black garlic, has several biological activities including antioxidant and anti-inflammatory effects, accounting for multiple beneficial roles, among which protection against insulin resistance is proposed herein. Despite these evidences, a mechanistic study supporting its direct involvement in modulating insulin response and in counteracting insulin resistance is still missing. The aim of this study is to evaluate the molecular mechanism of action of SAC in the insulin-dependent metabolic response. For this purpose, the effects of SAC on protein synthesis, glucose uptake, and GLUT4 translocation were assessed in C2C12 skeletal myotubes. The interaction of SAC with the insulin receptor was studied by molecular docking analyses and differential scanning calorimetry. Finally, the counteracting role of SAC against insulin resistance was studied in a C2C12 palmitic acid-induced insulin resistance model. Our results showed that SAC, like insulin, stimulates protein synthesis, glucose uptake and GLUT4 plasma membrane translocation in skeletal myotubes. These last effects were reduced in the presence of the insulin receptor antagonist S961. Moreover, docking and calorimetry results demonstrated the interaction of SAC with the insulin receptor kinase domain. Furthermore, SAC both prevents and reverses the development of palmitic acid-induced insulin resistance significantly, restoring glucose uptake to the levels detected in non-insulin-resistant cells. Altogether, these data provide mechanistic insights into the insulin-mimetic role of SAC, paving the way for future research on new compounds capable of preventing insulin resistance and the consequent onset of metabolic syndrome.

Received 2nd September 2025,
Accepted 18th October 2025

DOI: 10.1039/d5fo03746h

rsc.li/food-function

Introduction

Under physiological conditions, insulin regulates glucose metabolism in muscle, liver, and adipose tissue. The binding to its receptor (INSR) starts a signaling cascade that finely regulates glucose uptake from the blood into target cells.[1,2] In particular, the skeletal muscle is the primary site for the disposal of ingested glucose. During the postprandial phase, the increase in the plasma glucose concentration stimulates insulin secretion from the pancreas, and the consequent hyperglycemia induces glucose uptake in skeletal and cardiac muscle and adipose tissue.[3] The impaired response to insulin of target tissues, defined as insulin resistance (IR), entails the onset of metabolic-related dysfunctions, characterized by the inhibition of cellular glucose uptake, gluconeogenesis, lipolysis, and glycogenolysis.[1,2,4] Several diseases including type II diabetes mellitus (T2DM), cardiovascular disease, nonalcoholic fatty liver disease (NAFLD), and metabolic syndrome are clinically associated with IR.[5,6] Although the mechanisms underlying IR are not fully elucidated, several studies agree that lipid oversupply from high-fat, high-calorie nutrition or excessive adipose lipolysis could be the most common risk factor for developing IR. Indeed, adipose tissue in obese people releases pro-inflammatory cytokines and plasma free fatty acids (FFA), resulting in the accumulation of lipotoxic lipid metabolites, which contribute to the onset of IR.[2,3,7] The first approach in the prevention and treatment of IR is an

[a]*Department of Life Sciences and Systems Biology, University of Turin, Via Accademia Albertina 13, 10123 Turin, Italy. E-mail: mariapia.gallo@unito.it*
[b]*Department of Clinical and Biological Sciences, University of Turin, Regione Gonzole 10, 10043 Orbassano, Italy*
[c]*Biosfered S.r.l., Via Paolo Veronese 202, 10148 Turin, Italy*
[d]*Abel Nutraceuticals S.r.l., Via Paolo Veronese 202, 10148 Turin, Italy*
[e]*Department of Drug Science and Technology, University of Turin, Via P. Giuria 9, 10125 Turin, Italy*

intensive lifestyle modification. The Mediterranean Diet, as a hypocaloric scheme characterized by a daily consumption of vegetables, legumes, cereals, and extra virgin oil as the principal source of fat, is proven to be the best dietary approach with a considerable improvement of IR in obese patients.[8] Moreover, constant physical activity is recommended to enhance muscle insulin sensitivity.[9] The second, often necessary, is the pharmacological approach. The principal drugs like metformin, oral sulfonylureas, oral sodium-glucose cotransporter 2 (SGLT2) inhibitors, oral dipeptidyl peptidase 4 (DPP4) inhibitors, oral α-glucosidase, injectable glucagon-like peptide 1 (GLP1) receptor agonists, and injectable insulin currently prescribed for IR have the ultimate function of stimulating insulin secretion or increasing insulin sensitivity.[2] Besides this, in recent years, there has been a growing interest in plant-derived bioactive metabolites due to their potential protective and glucose metabolism-modulating properties. Among these, garlic (*Allium sativum*) has been one of the most studied dietary sources for health benefits. In particular, *S*-allyl cysteine (SAC) is the most abundant sulfur-containing compound present in black garlic (BG), a form of aged garlic obtained from raw garlic *via* the Maillard reaction under high-temperature and high-humidity conditions.[10] The antioxidant and anti-inflammatory activities of SAC are frequently reported in the literature,[11,12] and its anti-cancer,[13] anti-hepatotoxic,[14] anti-hypertensive,[15] and neuroprotective effects are also known.[12,16] We have previously demonstrated the protective effects of SAC on endothelial dysfunction, another important hallmark of metabolic syndrome, by increasing hydrogen sulfide (H_2S) and nitric oxide (NO) release.[17] Since the impact of SAC on glucose metabolism has so far only been studied *in vivo* in streptozotocin-induced diabetic rats,[18,19] this study aims to evaluate, at cellular and molecular levels, the effects of SAC on key elements of metabolic health and insulin pathway, using an *in vitro* model of skeletal muscle cells (C2C12). Moreover, building on a recent report[20] showing that a molecule closely related to SAC, S-Allylmercaptocysteine, can bind and activate the insulin receptor, we hypothesized a similar mechanism for SAC. To achieve the above-mentioned aims and explore this hypothesis, glucose uptake and GLUT4 (glucose transporter type 4) translocation were investigated, in both the presence and the absence of S961, an insulin receptor inhibitor. Moreover, the interaction of SAC with the insulin receptor was studied through molecular docking and differential scanning calorimetry (DSC). Finally, the potential role of SAC in preventing or reversing IR was evaluated in a C2C12 palmitate-induced insulin resistance model.

Materials and methods

Reagents

Unless otherwise specified, materials were obtained from Sigma Aldrich (Merck Group, Darmstadt, Germany). Plastics and reagents for cell cultures were obtained from Euroclone (Euroclone, Pero, Italy). 2-NBDG (2-(*N*-(7-nitrobenz-2-oxa-1,3-diazol-4-yl)amino)-2-deoxyglucose) for glucose uptake assay (code N13195), the cell permeant dye CellROX® Green Reagent for oxidative stress detection (code C10444), the Click-iT® Plus OPP Protein Synthesis Assay Kit (code C10456), and the rabbit polyclonal antibody against GLUT-4 (code PA5-23052) were obtained from Thermo Fisher Scientific (Thermo Fisher Scientific, Waltham, MA, USA). The CellTiter 96® AQueous One Solution Cell Proliferation Assay, based on the use of the tetrazolium compound [3-(4,5-dimethylthiazol-2-yl)-5-(3-carboxymethoxyphenyl)-2-(4-sulfophenyl)-2H-tetrazolium, inner salt] (MTS code G3580) was obtained from Promega Corp. (Madison, WI, USA).

The insulin receptor antagonist S961 (code 051-86) was purchased from Phoenix Pharmaceuticals Inc. (Burlingam, CA, USA). Antibodies for immunoblotting experiments were purchased from different providers: anti-AKT (pan) (C67E7) rabbit monoclonal (code 4691) and anti-p-AKT (Ser473) (D9E) XP® rabbit monoclonal (code 4060) were obtained from Cell Signalling Technology Inc. (Danvers, MA, USA); mouse monoclonal anti-β-actin (code A5316) was obtained from Merck/Sigma Aldrich; horseradish peroxidase-conjugated secondary antibodies were provided by Proteintech (Rosemont, IL, USA); and anti-rabbit (code SA00001-2) and anti-mouse (code 31430) antibodies were provided by Thermo Fisher Scientific.

Cell cultures

The mouse myoblast cell line C2C12 (ECACC 91031101, lot 17I044) was purchased from the European Collection of Authenticated Cell Cultures (ECACC, Salisbury, UK) and cultured in high-glucose Dulbecco's modified Eagle's medium (DMEM) supplemented with 10% fetal bovine serum (FBS), 1% penicillin/streptomycin, and 2 mM L-glutamine in a humidified atmosphere of 5% CO_2 at 37 °C. Cultures were plated at a density of 2×10^3 cells per cm^2 on tissue plastic dishes and sub-cultured before reaching 70% confluence. For all experiments, cells were seeded at a density of 10×10^3 cells per cm^2 on 96-well plates, coverslips, and glass bottom dishes (VWR Int., Radnor, PA, USA) to enhance adhesion. After cells reached confluence, differentiation was induced by changing the medium to DMEM supplemented with 2% horse serum (HS) for an additional five days. Except for the cell viability and ROS production assay, the day before the experiments, C2C12 cells were starved for 24 h in glucose and serum-free DMEM.

Crystal violet staining

Cellular viability was studied using crystal violet staining since MTT or similar assays could not be used due to chemical interference of reducing substances in the cellular medium (sulfhydryl-containing compounds such as SAC) with tetrazolium salts, as done in a previous work.[21] C2C12 cells were plated in 96–well plates at a density of 10×10^3 cells per cm^2 (3300 cells per well). Once differentiated, cells were treated with SAC at different concentrations (10 μM, 100 μM, 500 μM, 1 mM, and 10 mM) for 4 or 24 h, 16 wells for each condition as technical replicates. The effect on cell growth was estimated by staining

with crystal violet: cells were fixed in 2.5% glutaraldehyde in PBS for 20 min and then stained with crystal violet (0.1% in 20% methanol); the plates were allowed to dry, and then the dye was solubilized in acetic acid (10%, v/v) and the absorbance was read at 595 nm in a microplate reader (Infinite M Plex, Tecan Switzerland). Data were expressed as the percentages of absorbance referred to the control condition; the percentage values of three independent experiments (biological replicates) were then summarized and expressed as mean ± standard error of mean (SEM).

MTS assay

Cell viability following palmitate treatment was studied by CellTiter 96® AQueous One Solution Cell Proliferation Assay, since, unlike treatment with SAC, there were no problems of interference with the dye MTS. C2C12 cells were grown in 96-well plates as described for crystal violet staining; once differentiated, cells were treated with palmitate at different concentrations (0.25 mM, 0.5 mM, 0.75 mM, and 1 mM) for 24 h (16 wells for each condition as technical replicates). Then, the effect on cell viability was estimated by MTS staining: after removal of culture medium, 10 μL of MTS were added to 50 μL of fresh medium in each well, followed by 30 minutes of incubation at 37 °C. During this time, MTS was bioreduced by metabolically active cells into a soluble and colored formazan product, whose absorbance, directly proportional to the number of viable cells, was read at 490 nm using an Infinite M Plex microplate reader. Data were expressed as percentages of absorbance referred to the control condition; percentage values of four independent experiments (biological replicates) were then analyzed to calculate mean ± SEM.

Reactive oxygen species (ROS)

C2C12 cells, grown on 96-well black plates at a density of 10×10^3 cells per cm^2 (3300 cells per well), once differentiated were pretreated with 20 μM menadione (as a positive control) for 1 h alone or in combination with 100 μM SAC for 30 min (16 wells for each condition as technical replicates); the cells were loaded with 5 μM CellROX® green probe for the last 30 min in the dark. Then, the cells were washed two times with PBS, and the fluorescence was acquired using a microplate reader (Infinite M Plex) at $485_{Ex}/520_{Em}$ nm. The fluorescence intensity was expressed in percentage as the mean value of the resulting fluorescence for each condition compared to the control of three independent experiments (biological replicates) ± SEM. In another set of experiments, the effect of palmitate on ROS production was examined. Cells were grown as before on 96-well black plates, and after differentiation, two lanes (16 wells as technical replicates) were treated with 0.75 mM palmitate for 24 h. Next, two lanes were treated with 20 μM menadione (as a positive control) for 1 h; the cells were loaded with 5 μM CellROX® green probe for the last 30 min in the dark and the microplates were processed as described above. The fluorescence intensity was expressed in percentage as the mean value of the resulting fluorescence for each condition compared to the control; four independent experiments (biological replicates) were performed.

Glucose uptake measurements

Differentiated C2C12 cells plated in black clear-bottom 96-well plates (10×103 cells per cm^2) were starved for 24 h in DMEM glucose and serum-free medium. Cells were treated with 100 μM SAC and simultaneously loaded with 100 μM of 2-NBDG in glucose and serum-free DMEM for 30 min in the dark (16 wells for each condition as technical replicates). Insulin (100 nM) was used as a positive control. For the experiments, with the insulin receptor inhibitor (S961), cells were treated with 100 μM SAC or 100 nm insulin for 30 min, in combination or not with 10 nM S961 (60 min). After two washes in PBS, the cells were lysed with a buffer containing 0.1 M KH_2PO_4 and 1% Triton X-100, pH 10, and the fluorescence intensity was recorded using a microplate reader (Infinite M Plex) at $465_{Ex}/540_{Em}$ nm. The fluorescence intensity was expressed in percentage as the mean value of the resulting fluorescence for each condition compared to the control of three independent experiments (biological replicates) ± SEM. For live cell imaging, cells were plated in glass-bottom dishes (10×10^3 cells per cm^2) and differentiated. The treatment was carried out as described above. After two washes in PBS, the cells were directly observed in confocal microscopy. The fluorescence images were acquired using a confocal microscope (Leica Stellaris 5, Leica Microsystems, Germany) at 488 nM with a 60× Uplan FI (NA 1.25) oil-immersion objective. Fluorescence variations were calculated by defining and measuring regions of interest (ROIs) using the ImageJ software.

Protein synthesis assay

Differentiated C2C12 cells plated in glass-bottom dishes (10×10^3 cells per cm^2) were treated with 100 μM SAC or 100 nM insulin for 60 min in glucose and serum-free DMEM. Then, a Click-iT® Plus OPP Protein Synthesis Assay Kit was used following the protocol. Briefly, after the initial incubation with a Click-iT® OPP working solution, cells were fixed for 15 min in 4% paraformaldehyde and permeabilized with PBS 0.5% Triton for 15 min. Then, the Click-iT® Plus OPP reaction cocktail was added, and the HCS NuclearMask™ Blue Stain was performed. Finally, nascent protein synthesis was assessed by measuring the signal intensity by confocal microscopy (Leica Stellaris 5) at 488 nm. For the quantification analysis, ten independent fields of each experimental condition were analyzed using the ImageJ software, using the '3D object counter' tool. Biological replicates were performed three times.

GLUT4 translocation

Differentiated C2C12 cells plated on glass coverslips (10×103 cells per cm^2) were starved for 24 h in glucose and serum-free DMEM. Cells were treated with 100 μM SAC or 100 nM insulin for 30 min in combination or not with 10 nM S961 (60 min) in glucose and serum-free DMEM. Then cells were fixed for 40 min in 4% paraformaldehyde dissolved in 0.1 M phosphate

buffer, pH 7.3. After three washes with PBS, cells were incubated for 20 min with 0.3% Triton and 1% bovine serum albumin in PBS and stained for 24 h at 4 °C with the primary polyclonal antibody anti-GLUT4 in a ratio of 1/100. Cover slides were washed twice with PBS and incubated for 1 h at room temperature with the secondary antibody, anti-rabbit Alexa Fluor 568 (Thermo Fisher Scientific) in a ratio of 1/1000. After two washes in PBS, coverslips were mounted on standard slides with DABCO and observed using a confocal microscope (Leica Stellaris 5). GLUT4 staining measurements of both the cell periphery and the cell interior were performed using the ImageJ software. Briefly, for each myotube, the enlarged plugin was employed to design an ROI band of 5 μm around the plasma membrane, and the fluorescence intensities of both the band and the cellular inside were collected.

The data from three independent experiments were expressed as peripheral/internal fluorescence and summarized to calculate mean ± SEM.

Immunoblotting

C2C12 cells were seeded on plastic dishes, 20 cm^2 of growth area, at a density of 10×10^3 cells per cm^2 in 10% FCS DMEM, and, after differentiation in DMEM + 2%HS, the cells were starved for 24 h in glucose and serum-free DMEM. Cells were then treated with 100 nM insulin or 100 μM SAC for 30 min. Cell monolayers were lysed in 200 μL of RIPA lysis buffer (Thermo Fisher Scientific) containing a phosphatase inhibitor cocktail (PhosSTOP, Roche, Mannheim, Germany) forced through a 1 mL syringe needle and centrifuged at 10 000 rpm for 5 min at 4 °C. Proteins (30 μg per lane) were resolved on 12% SDS-PAGE, transferred onto a polyvinylidene fluoride (PVDF) membrane, (Thermo Fisher Scientific) in a cold transfer buffer (25 mM Tris pH 8.3, 192 mM glycine, 0.1% SDS, 20% methanol) and blocked for 1 h at 37 °C in TBST (10 mM Tris pH 7.5, 0.1 M NaCl, 0.1% Tween 20) plus 5% non-fat dry milk. Blots were incubated overnight at 4 °C with primary antibodies (1 : 1000 rabbit monoclonal anti-AKT and anti-pAKT; 1 : 2000 mouse monoclonal anti-β-actin) in TBST containing 1% non-fat dry milk. Membranes were then washed three times in TBST with weak shaking and incubated for 1 h at room temperature with secondary antibodies (anti-rabbit, 1 : 10.000; anti-mouse, 1 : 20.000) in TBST containing 1% non-fat dry milk, followed by a second set of three washes with TBST. Bands were visualized by chemiluminescence with Western Lightning Plus-ECL (PerkinElmer, Waltham, MA, USA). The protein levels were determined using the ImageJ software; for each condition, the ratio of p-AKT/AKT was evaluated and then normalized against INS as a positive control. The comparison of the β-actin band intensity ensured equal protein loading. The results of $n = 6$ independent experiments (biological replicates) were averaged and expressed in percentage as mean ± SEM.

Mouse insulin receptor

The protein kinase domain (Leu1067–Gly1296) of the Mouse Insulin Receptor, UniProt ID: Q9WTL4, was purchased from Abbexa (Milton, Cambridge CB4 0GJ, UK) in a lyophilized form. The pre-lyophilization buffer consisted of PBS, pH 7.4, containing 0.01% sarcosyl and 5% Trehalose. The protein concentration was 13.8 μM after reconstitution.

Differential scanning calorimetry (DSC)

The DSC experiments were conducted using a VP-Capillary DSC (Malvern Instruments Ltd Worcestershire, UK), as reported previously.[22,23] The protein was analyzed in the absence and presence of 150 μM SAC. Each sample was pre-incubated at 25 °C for 10 minutes before the run in a water bath, 200 μL of sample was placed in the cell and then 200 μL of PBS buffer was placed in the reference cell. The temperature was increased from 25 °C to 90 °C at a 90 °C h^{-1} scan rate after an equilibration of 10 minutes at 25 °C. Data analysis was performed using Origin.

In silico molecular docking studies

The three-dimensional structure of the tyrosine kinase receptor of the human insulin receptor was obtained from the RCSB database, PDB ID: 2AUH.[24] 2AUH contains the insulin receptor tyrosine kinase in complex with Grb14, so the coordinates Grb14 were removed from the PDB file. Molecular docking was performed using the YASARA (10.1093/bioinformatics/btu426) structure, version 23.9.9, operating under Windows 11 Pro an HP OMEN 880–102 nL workstation (Intel Core i7-8700K, 2.8 GHz CPU, and 1 GB memory). The 3D structure of SAC was downloaded as an .sdf file from PubChem, energy minimized with YASARA, and saved as the .pdb file. Docking of each ligand to the "receptor" file was carried out using the YASARA-embedded AutoDock VINA algorithm[25] by using the "dock_run.mcr" macro exploiting 999 runs. The YASARA macro performs structure preparation of the ligand, docking to the receptor, and results sorting by binding energy/predicted binding affinity. In YASARA, results are ranked by binding energy, where more positive energies indicate stronger binding and negative energies equate to no binding.[26] Best poses were to predict the most probable binding site between the protein and the ligand.

Palmitic acid preparation and treatments

A palmitic acid (PA) solution was prepared according to Sun *et al.*[27] Briefly, sodium palmitate powder (100 mM) was dissolved in H_2O by heating for 10 min at 70 °C with agitation using a thermomixer, and bovine serum albumin (BSA) was dissolved in H_2O to a concentration of 10% (wt/vol) at 55 °C with agitation. Then, equal volumes of the two solutions (1 : 1) were mixed to obtain a 50 mM stock solution and stored at −20 °C. The cells were treated with 0.75 mM PA for 16 h in glucose and serum-free DMEM alone or in combination with 100 μM SAC. In the last 30 min, cells were stimulated with 100 nM insulin or 100 μM SAC and simultaneously loaded with 100 μM of 2-NBDG in glucose and serum-free DMEM (16 wells for each condition as technical replicates), as explained above.

Statistical analysis

Data are expressed as mean ± standard error of the mean (SEM); statistical analyses were performed using ANOVA (one-way analysis of variance) followed by Bonferroni's multiple comparison test. Differences with $p < 0.05$ were considered statistically significant.

Results

SAC does not affect C2C12 cells' viability and has antioxidant activity on menadione-treated cells

To initially assess the effect of SAC on cell viability, C2C12 cells were treated with increasing concentrations of the molecule (10–100–500 μM, 1–10 mM) for 4 and 24 hours, and then crystal violet staining was performed. As shown in Fig. 1A, SAC has no significant impact on C2C12 cell viability at any tested concentration after 4 hours of exposure; a reduction in cell viability is only observed with the highest concentration (10 mM) after 24 hours of treatment (Fig. 1B). Thus, the following experiments were performed with 100 μM SAC, which showed no cytotoxic effects at either of the time points tested. In addition to the cell viability tests, further experiments were conducted to verify the antioxidant activity of SAC in our cellular model using the CellROX® green probe. The cells were pre-treated with 20 μM menadione (MEN), a known inducer of reactive oxygen species (ROS), for 1 hour either alone or in combination with 100 μM SAC (30 minutes). As expected, MEN leads to increased fluorescence, indicating an enhancement in intracellular ROS production. In contrast, SAC alone does not affect the ROS concentration but significantly reduces the increase in ROS production induced by MEN. These results highlight a protective role of SAC against oxidative stress in C2C12 cells (Fig. 1C).

SAC enhances insulin signalling, glucose uptake, and protein synthesis in C2C12 skeletal muscle cells

Although some studies highlighted a protective role of SAC or astaxanthin-SAC diester in both Streptozotocin-induced diabetic rats or pancreatic beta cell lines, there are no data on the direct cellular mechanisms by which SAC could affect glucose and protein metabolism in insulin-dependent tissues.[18,28,29] Given these premises, our aim was to evaluate the effect of SAC on key parameters of the insulin response in skeletal muscle, such as AKT phosphorylation, a key protein in the insulin signalling cascade, glucose uptake, and protein synthesis, by using the C2C12 cellular model. First, western blot experiments were conducted to evaluate the effect of 100 μM SAC on p-AKT. As shown in Fig. 2A and B, after 30 min treatment with SAC, AKT phosphorylation is significantly increased compared to the control condition. Given these results, the glucose uptake was assessed following a 30-minute treatment with the positive control insulin (100 nM) and SAC (100 μM) using the 2-NBDG fluorescent glucose analog. As shown in Fig. 2C and D, SAC significantly increases the fluorescence intensity, indicating an enhanced glucose uptake, comparable to what is observed with insulin. Next, the impact of SAC on protein synthesis was evaluated using a Click-iT® Plus OPP Protein Synthesis Assay Kit, which allows the staining of newly translated proteins. As can be observed in the representative images (Fig. 2E) and the corresponding quantification graph (Fig. 2F), SAC can stimulate de-novo protein synthesis similarly to insulin after a 60-minute treatment.

SAC-mediated effects on glucose uptake and GLUT4 translocation are reduced by the insulin receptor antagonist S961

Given these preliminary results about the insulin-like behavior of SAC on glucose uptake and protein synthesis, we wondered

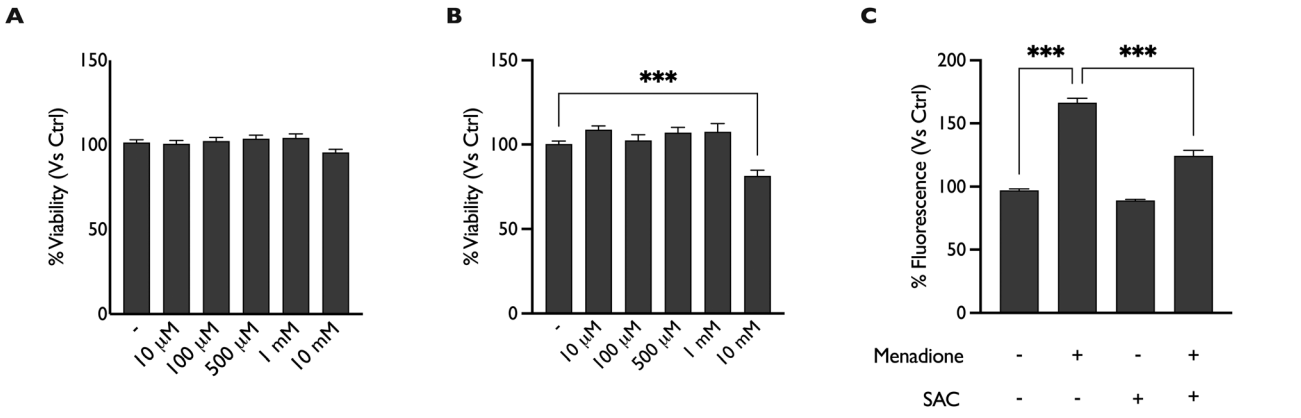

Fig. 1 Effect of SAC on C2C12 cellular viability and ROS production. (A and B) Bar graph summarizing the effect on the cellular viability of increasing concentrations of SAC (10–100–500 μM and 1–10 mM) after 4 (A) or 24 (B) hours of treatment. Crystal violet absorbance was read at 595 nm. (C) Bar graph summarizing the effect on ROS production in menadione-treated cells (20 μM and 1 hour) alone or in combination with SAC (100 μM and 30 minutes) loaded with CellROX® green probe (5 μM and 30 minutes). Fluorescence was evaluated using a microplate reader ($485_{Ex}/520_{Em}$ nm). Data in percentage referred to the control condition of $n = 3$ independent experiments are represented as mean ± SEM. ***$p < 0.001$ (ANOVA followed by the Bonferroni *post hoc* test). The values are as follows: (A) Ctrl: 101.28 ± 1.62; 10 μM: 97.28 ± 1.50; 100 μM: 98.53 ± 1.43; 500 μM: 100.57 ± 1.82; 1 mM: 100.11 ± 1.85; and 10 mM: 92.02 ± 1.34. (B) Ctrl: 100.28 ± 1.78; 10 μM: 108.81 ± 2.25; 100 μM: 102.38 ± 3.40; 500 μM: 107.06 ± 3.17; 1 mM: 107.60 ± 4.84; and 10 mM: 81.59 ± 3.29. (C) Ctrl: 97.07 ± 1.24; MEN: 166.38 ± 3.47; SAC: 89.16 ± 0.84; and MEN + SAC: 124.32 ± 4.31.

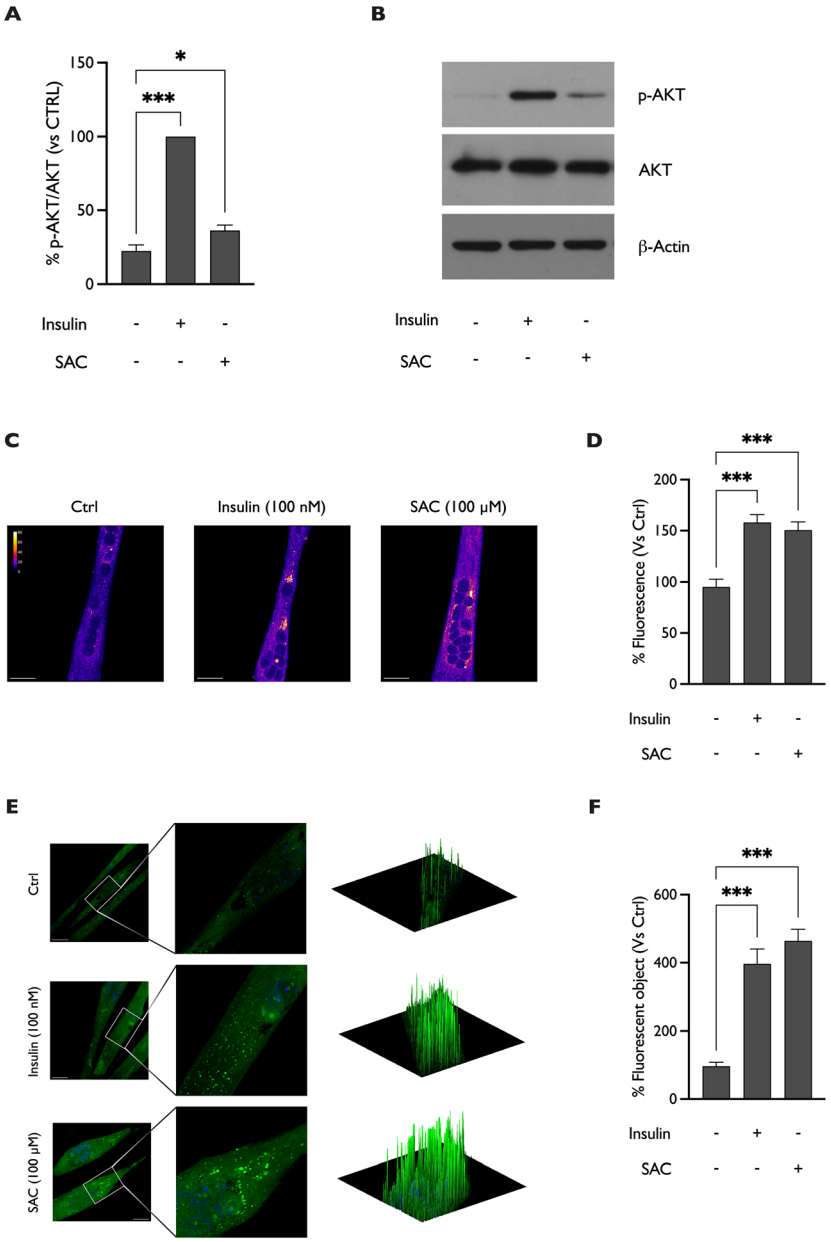

Fig. 2 Effect of SAC on insulin signalling, glucose uptake and protein synthesis. (A) Bar graph summarizing the p-AKT/AKT ratio normalized toward positive control (insulin) after treatment with 100 nM of insulin (30 minutes) and 100 μM of SAC (30 minutes). Data in percentage of n = 6 independent experiments are represented as mean ± SEM. *p < 0.5 (CTRL *vs.* SAC p = 0.024), ***p < 0.001 (ANOVA followed by the Bonferroni *post hoc* test). The values are as follows: Ctrl: 22.55 ± 4.16; Ins: 100.00 ± 0.00; and SAC: 36.31 ± 3.64. (B) Representative western blot experiment showing the effect of insulin and SAC on AKT phosphorylation. Comparison of β-actin intensity ensured equal protein loading. (C) Representative images of C2C12 cells loaded with 100 μM 2-NBDG for 30 minutes and treated with insulin (100 nM and 30 minutes) or SAC (100 μM and 30 minutes). Scale bars: 30 μm. Confocal microscopy images (60×) are presented in pseudocolor (LUT = fire) to better show the fluorescence intensity variations. (D) Summarizing graph of the enhanced glucose uptake after stimulation with both insulin and SAC under the same condition described in (A). No significant differences were observed between insulin and SAC stimulation. Fluorescence was evaluated using a microplate reader ($465_{Ex}/540_{Em}$ nm). (E) Representative images (60×) of C2C12 at normal (left) or higher (right) magnification of the staining with the Click-iT® Plus OPP reaction cocktail (green spots). Nuclei were marked with NuclearMask™ Blue Stain. A higher number of spots are present in cells treated with insulin (100 nM and 60 minutes) and SAC (100 μM and 60 minutes), thus suggesting a role of SAC in enhancing protein synthesis. Scale bars: 30 μm. Differences in marked spots between control and treatments are also represented in a 3D surface plot model. (F) Bar graph summarizing the quantification of marked spots following insulin and SAC treatment under the same conditions described in (E). For each experiment, ten independent fields of each experimental condition were analyzed using the ImageJ software. No significant differences were observed between insulin and SAC stimulation. Data in percentage referred to the control condition of n = 3 independent experiments are represented as mean ± SEM. ***p < 0.001 (ANOVA followed by the Bonferroni *post hoc* test). The values are as follows: (D) Ctrl: 95.27 ± 7.49; Ins: 158.10 ± 7.63; and SAC: 150.57 ± 8.02. (F) Ctrl: 96.56 ± 11.87, n cells = 27; Ins: 396.77 ± 43.33, n cells = 25; and SAC: 464.14 ± 34.35, n cells = 24.

whether this effect might be modulated by direct binding to the insulin receptor. This hypothesis was based on previous findings by Luo *et al.*, who demonstrated that S-Allylmercaptocysteine , another molecule extracted from black garlic, directly interacts with the insulin receptor in the binding site for the growth factor receptor binding protein 14 (GRB14), thus disrupting its inhibitory interaction with the receptor tyrosine kinase domain.[20] To verify the potential involvement of the insulin receptor in the modulation of SAC activities in C2C12 cells, we performed glucose uptake measurements and GLUT4 translocation from the cytoplasm to the plasma membrane with the immunofluorescence staining, in the presence of the insulin receptor antagonist S961. Cells were treated with insulin (100 nM) or SAC (100 μM) for 30 minutes, either alone or in combination with S961 (10 nM and 1 hour). As shown in Fig. 3A and B, co-treatment with S961 significantly reduces the glucose uptake induced by both insulin and SAC treatment alone. Moreover, while GLUT4 translocation is promoted by both insulin and SAC treatment, the co-treatment with S961 significantly reduced these effects, restoring the GLUT4 membrane levels to near the control one (Fig. 3C and D). Taken together, these results support the hypothesis of the involvement of insulin receptor in mediating the SAC effect on glucose metabolism.

This was also confirmed by *in silico* experiments with molecular docking. Clustering analysis of the top 20 docking poses, based on binding energy values calculated using AutoDock Vina, revealed a consistent cluster centered around 4.9 kcal mol^{-1}, suggesting a preferred binding site for SAC. The residues most frequently involved in SAC binding include R1039, I1042, E1043, R1131, M1153, R1155, Y1163, K1165, G1169, L1170, and L1171 with pY1163 (phosphotyrosine) present in 19 out of 20 top poses.

pY1163 is a known site of post-translational modification involved in insulin receptor activation and regulation. Its interaction with SAC suggests potential competitive binding with endogenous regulators such as GRB14 and PTP1B. The identified binding region partially overlaps with the GRB14 binding site (Fig. 3E and F) reported in the crystal structure (PDB ID: 2AUH), which involves R1131, E1134, D1150, Y1163, K1165, G1169, and L1170.[24] This area also includes key residues of the activation loop (A-loop), particularly Y1158, Y1162, and Y1163, whose phosphorylation is essential for kinase activation. The docking results suggest that SAC may partially and dynamically displace GRB14 from the kinase domain, without inducing its complete dissociation. Such an effect could hinder access by PTP1B to phosphotyrosines, thereby contributing to the transient maintenance of receptor phosphorylation and activation. The moderate binding energy (~4.9 kcal mol^{-1}) suggests a transient or reversible interaction, consistent with a non-covalent regulatory effect. Additionally, the predicted hydrogen bonds are primarily located in the peripheral regions of the catalytic core, supporting the hypothesis that SAC binding could induce local destabilization of the kinase domain without directly occluding the active site.

SAC modulates conformational stability of insulin receptor kinase domain

Differential scanning calorimetry (DSC) was employed to investigate the thermal stability of the insulin receptor kinase domain (INSR) in the absence and presence of the ligand SAC. In the absence of ligand (Fig. 4, black line), the protein showed a melting temperature of 66.8 °C. The shape and sharpness of the thermogram clearly indicate a well-folded cooperative unfolding transition, consistent with a compact and thermodynamically stable conformation. The unfolding process is irreversible, as rescan did not result in the formation of any detectable peak.

Upon addition of 150 μM SAC, the melting temperature shifted to 58.7 °C (Fig. 4, red line), indicating ligand-induced destabilization of the overall protein fold, as also indicated by a T_{onset} decrease from 50 °C to 38 °C and the enlargement of the peak. This behavior suggests that SAC interacts with the receptor, altering its conformational equilibrium, increasing local flexibility, and resulting in the destabilization of the structure. This effect is consistent with the hypothesis that SAC binds near the activation loop (A-loop), modulating its conformational stability in the absence and presence of the ligand. Moreover, in this case, the unfolding process is irreversible.

Palmitic acid did not affect cellular viability and ROS production

To investigate if SAC specifically counteracts palmitate-induced insulin resistance by activating the insulin pathway, rather than acting through a general cytoprotective/antioxidant mechanism, we evaluated the viability of C2C12 treated for 24 h at different concentrations of palmitic acid (PA) (from 0.25 mM to 1 mM). As shown in Fig. 5A, PA did not affect C2C12 viability at any of the tested concentrations. Moreover, the changes in intracellular ROS production were evaluated, using the CellROX® green probe. While the positive control menadione (20 μM, 30 min), as expected, significantly increased ROS production in comparison to the control condition, treatment with 0.75 mM PA for 24 hours did not enhance the fluorescence intensity and so ROS release (Fig. 5B) in our cellular model.

SAC prevents palmitic acid-induced insulin resistance in C2C12 myotubes

On the basis of the previous findings, we hypothesized a potential role of SAC in preserving the insulin receptor function under conditions of an impaired insulin receptor activation, *i.e.* in insulin resistance. To investigate this mechanism, we first developed an *in vitro* protocol to generate insulin-resistant C2C12 cells. Elevated plasma levels of free fatty acid (FFA) are well known to have an essential role in the pathogenesis of insulin resistance in skeletal muscle.[30] Among them, palmitic acid (PA) is the most commonly used inducer of insulin resistance in *in vitro* models.[31] Differentiated C2C12 cells were treated with 0.75 mM PA for 16 hours alone or in

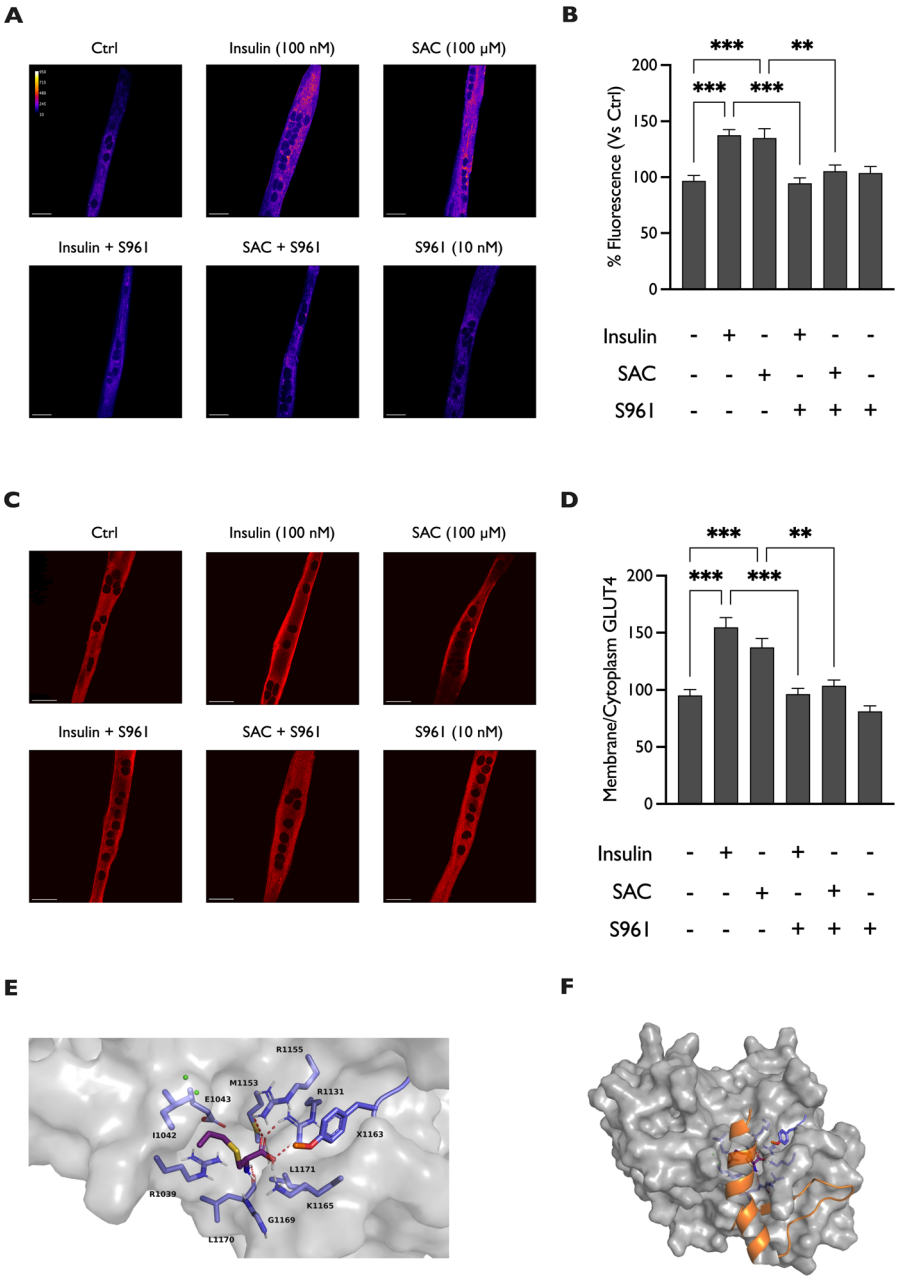

Fig. 3 Interaction with the insulin receptor mediates SAC effects. (A) Representative confocal microscopy images of C2C12 cells loaded with a 100 µM 2-NBDG probe for 30 minutes and treated with insulin (100 nM and 30 minutes) and SAC (100 µM and 30 minutes) alone or in combination with S961 (10 nM, 1 hour). Scale bars: 30 µm. Confocal microscopic images (60×) are presented in pseudocolor (LUT = fire) to better show the fluorescence intensity variations. (B) Bar graph showing the reduction in glucose uptake after S961 co-treatment with insulin or SAC under the same experimental condition described in (A). No significant differences were observed between insulin and SAC stimulation. Fluorescence was evaluated using a microplate reader ($465_{Ex}/540_{Em}$ nm). Data in percentage referred to the control condition of $n = 3$ independent experiments are represented as mean ± SEM. $^{**}p < 0.01$ (SAC *vs.* SAC + S961 $p = 0.009$), $^{***}p < 0.001$, (ANOVA followed by the Bonferroni *post hoc* test). (C) Representative confocal microscopy images (60×) of GLUT4 immunofluorescence staining. After insulin (100 nM) and SAC (100 µM) 30-minute treatment, the fluorescence signal is localized to the peripheral plasmalemma, thus suggesting the GLUT4 translocation, while following the co-treatment with S961, the signal is prevalently cytoplasmic, similar to the control condition. Scale bars: 30 µm. (D) Bar graph summarizing the quantification of GLUT4 translocation using the ImageJ software (see Methods for details). Fluorescence was detected at 568 nm. For each experiment, ten independent fields of each experimental condition were analyzed. No significant differences have been observed between insulin and SAC stimulation. Data in percentage referred to the control condition of $n = 3$ independent experiments are represented as mean ± SEM. $^{**}p < 0.01$ (SAC *vs.* SAC + S961 $p = 0.006$), $^{***}p < 0.001$, (ANOVA followed by the Bonferroni *post hoc* test). (E) Visual representation of the docking poses clusterization, where hydrogen bonds are shown in red. (F) Spatial visualization of the SAC binding cleft on INSR, highlighting the GRB14 interaction (orange alpha helical domain). The values are as follows: (B) Ctrl: 96.77 ± 4.82; Ins: 137.54 ± 5.10; SAC: 135.12 ± 8.22; Ins + S961: 94.59 ± 4.83; SAC + S961: 105.41 ± 5.48; and S961: 103.75 ± 5.85. (D) Ctrl: 95.05 ± 5.23, *n* cells = 31; Ins: 154.69 ± 8.51, *n* cells = 35; SAC: 137.40 ± 7.46, *n* cells = 29; Ins + S961: 96.42 ± 5.06, *n* cells = 35; SAC + S961: 103.80 ± 4.88, *n* cells = 29; and S961: 81.26 ± 4.89, *n* cells = 20.

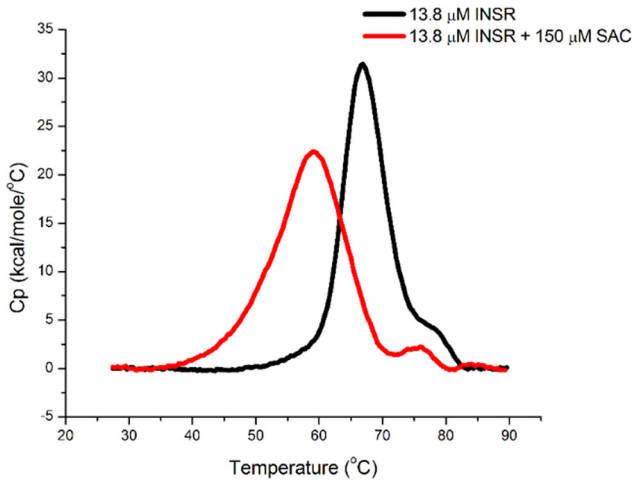

Fig. 4 Thermograms of INSR in the absence of SAC (black) and with 150 μM of SAC (red).

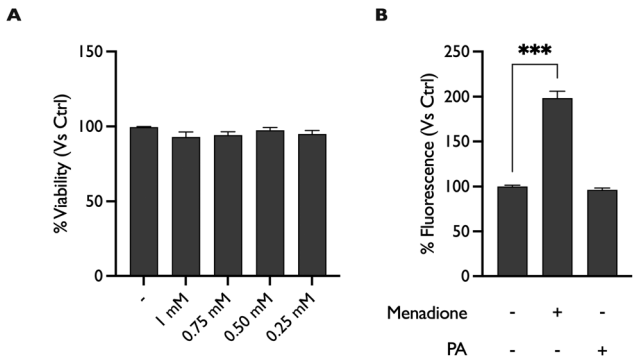

Fig. 5 Palmitic acid did not affect the cellular viability and ROS production in C2C12 cells. (A) Bar graph summarizing the effect on the cellular viability of increasing concentrations of palmitic acid (0.25–0.50–0.75–1 mM) after 24 hours of treatment. The absorbance was read at 490 nm. (B) Bar graph summarizing the effect on ROS production in menadione-treated cells (20 μM and 1 hour) or palmitic acid-treated cells (0.75 mM and 24 hours) loaded with a CellROX® green probe (5 μM and 30 minutes). Fluorescence was evaluated using a microplate reader ($485_{Ex}/520_{Em}$ nm). Data in percentage referred to the control condition of n = 4 independent experiments are represented as mean ± SEM. ***p < 0.001 (ANOVA followed by the Bonferroni *post hoc* test). The values are as follows: (A) Ctrl: 99.60 ± 0.28; 1 mM: 92.93 ± 3.38; 0.75 mM: 94.12 ± 2.37; 0.50 mM: 97.39 ± 1.96; and 1 mM: 94.87 ± 2.49. (B) Ctrl: 100.00 ± 1.50; MEN: 198.50 ± 7.67; and PA: 96.41 ± 2.10.

combination with 100 μM SAC. Cells were then treated or not with insulin (100 nM) and loaded with the 2-NBDG probe in the last 30 minutes (Fig. 6A). As shown in Fig. 6B and C, cells have become insulin resistant after 16 hours of PA treatment, as evidenced by their impaired response to acute insulin stimulation compared to cells untreated with PA. However, the addition of SAC together with PA (16 h) prevents this condition, as cells respond to an acute insulin pulse; indeed, the levels of insulin-induced glucose uptake are significantly higher in 16 h PA + SAC-treated cells with respect to only 16 h PA-treated cells, suggesting that SAC could prevent the establishment of insulin resistance.

SAC reverses insulin resistance in palmitic acid-treated C2C12 myotubes

Given the role of SAC in preventing PA-induced insulin resistance following a 16-hour treatment, we also investigated a potential role of the molecule in exerting an acute reversion of the insulin resistance state. To test this mechanism, C2C12 cells were treated with 0.75 mM PA for 16 hours. Then, the cells were then treated or not for 30 min with insulin (100 nM) or SAC (100 μM) and loaded with the 2-NBDG probe (Fig. 7A). As shown in representative images and expressed in the summarizing graph (Fig. 7B and C), in PA-treated cells, SAC restored the glucose uptake extent to the level detected in non-insulin-resistant cells treated with insulin or SAC. This suggests that SAC, in addition to preventing insulin resistance, could also reverse an established downregulation of insulin response if acutely applied to insulin-resistant myotubes.

Discussion

The present work investigates the effect of *S*-allyl cysteine (SAC), a bioactive compound found in black garlic and black garlic extracts for dietary supplements, on key aspects of metabolic health and insulin pathway using an *in vitro* model of skeletal muscle cells (C2C12). Specifically, this research presents the following three main findings: first, we found that SAC enhances insulin signalling, glucose uptake, and protein synthesis in C2C12 skeletal muscle cells. Second, we demonstrated that SAC interacts with the insulin receptor kinase domain, thus enhancing glucose uptake and GLUT4 translocation to the plasma membrane. Finally, we showed that SAC prevents and reverses insulin resistance in palmitic acid-induced insulin-resistant myotubes.

To date, *in vivo* and *in vitro* studies have mainly focused on the antioxidant and anti-inflammatory effects of SAC. Indeed, Saravan and Ponmurugan reported in their study on streptozotocin-induced diabetic rats that SAC prevented the increased levels of lipid peroxidation markers, reduced reactive oxygen free radicals, and improved the activities of tissue antioxidant enzymes.[18,19] Instead, Gupta *et al.* demonstrated that SAC protected C2C12 skeletal muscle cells from H_2O_2-induced atrophic effects by decreasing the ROS levels, lipid peroxidation, and cytokine levels.[32] Our study on the antioxidant effect of SAC is in accordance with these works, as 100 μM SAC (30 minutes) significantly reduces the increase in ROS production induced by menadione, highlighting a protective role of SAC against oxidative stress on C2C12 cells (Fig. 1C). Besides the well-known antioxidant and anti-inflammatory activities of SAC, to our knowledge, there are no data on the direct cellular mechanisms by which SAC could affect glucose and protein metabolism in insulin-dependent tissues, in particular in skeletal muscle. To verify the possible involvement of SAC in modulating glucose metabolism, we first analyzed the

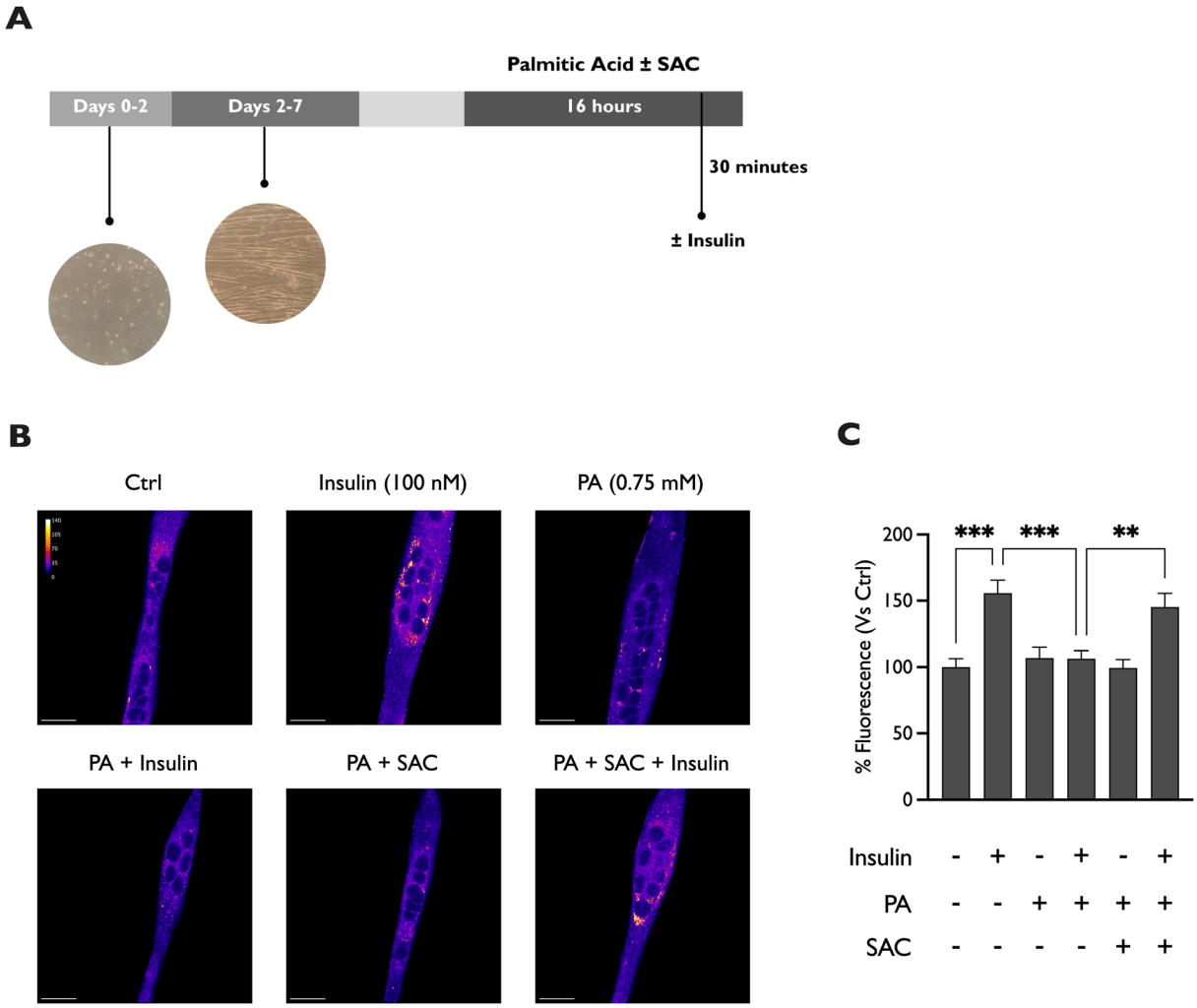

Fig. 6 SAC prevents the condition of insulin resistance in palmitic acid-treated C2C12 cells. (A) Experimental timeline. C2C12 cells were treated with PA (0.75 mM) for 16 hours alone or in combination with SAC (100 μM). In the last 30 minutes, cells were treated or not with insulin (100 nM) and loaded with a 2-NBDG probe. (B) Representative confocal microscopic images of C2C12 cells loaded with a 100 μM 2-NBDG probe for 30 minutes and treated with palmitate (0.75 mM and 16 hours) ± SAC (100 μM and 16 hours) and ±insulin (100 nM and 30 minutes). Scale bars: 30 μm. Confocal microscopic images (60×) are presented in pseudocolor (LUT = fire) to better show the fluorescence intensity variations. (C) Bar graph summarizing the effect of PA and the prevention with SAC in insulin-resistant cells under the same experimental condition described in (B). Fluorescence was evaluated using a microplate reader ($465_{Ex}/540_{Em}$ nm). Data in percentage referred to the control condition of n = 3 independent experiments are represented as mean ± SEM. $^{**}p < 0.01$ (insulin + PA *vs.* insulin + PA + SAC $p = 0.008$), $^{***}p < 0.001$ (ANOVA followed by the Bonferroni *post hoc* test). The values are as follows: (C) Ctrl: 100.00 ± 6.49; Ins: 155.78 ± 9.82; PA: 106.88 ± 8.04; PA + Ins: 106.45 ± 5.91; PA + SAC: 99.47 ± 6.31; and PA + SAC + Ins: 145.25 ± 10.33.

impact of SAC on the insulin signalling pathway, performing western blot analyses for p-AKT. As shown in Fig. 2A and B, SAC significantly enhances AKT phosphorylation in comparison to non-treated cells. We then conducted glucose uptake experiments using the 2-NBDG fluorescent glucose analog (Fig. 2C and D). It was found that 100 μM SAC significantly enhanced glucose uptake in a similar way to what we observed with 100 nM insulin. Moreover, we evaluated the effect of SAC on the *de novo* protein synthesis, using a Click-iT® Plus OPP Protein Synthesis Assay Kit. SAC was able to stimulate protein synthesis similarly to insulin after a 60-minute treatment (Fig. 2E and F). Given these preliminary results, we wondered if the insulin-like behavior of SAC might be modulated by direct binding to the insulin receptor. In a previous study, Luo *et al.* have demonstrated that S-Allylm, another molecule highly present in black garlic, directly interacts with the insulin receptor in the binding site for the growth factor receptor binding protein 14 (GRB14), disrupting its inhibitory interaction with the receptor tyrosine kinase domain.[20] To verify our hypothesis, we performed glucose uptake and GLUT4 staining experiments in the presence or absence of the insulin receptor inhibitor S961. In 10 nM S961-treated cells, both glucose uptake and GLUT4 translocation are significantly reduced when stimulated with 100 μM SAC or 100 nM insulin,

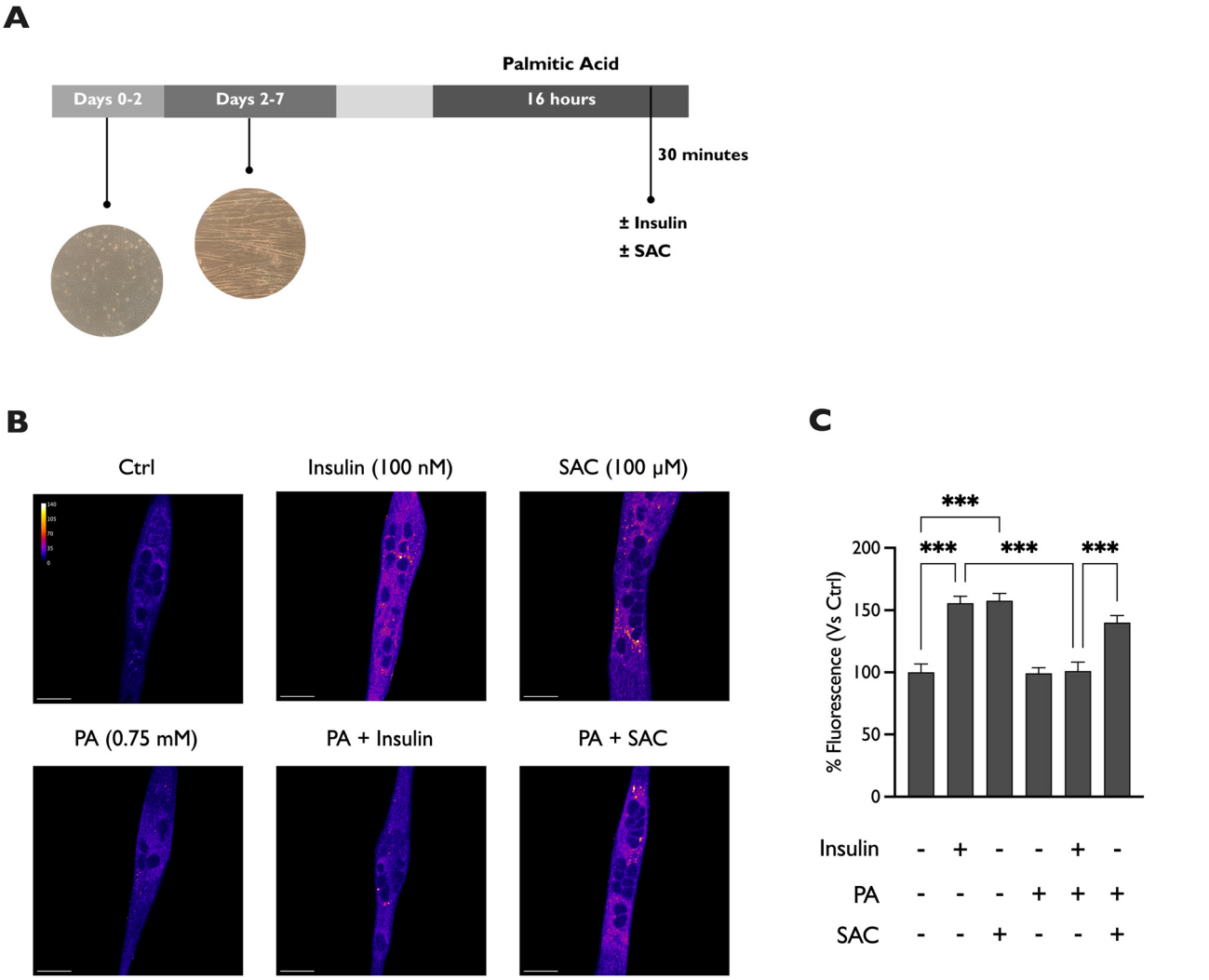

Fig. 7 SAC reverts an insulin-resistance condition in the palmitic acid-treated C2C12 cells. (A) Experimental timeline. C2C12 cells were treated with PA (0.75 mM) for 16 hours. In the last 30 minutes, cells were treated or without insulin (100 nM) and SAC (100 µM) and loaded with the 2-NBDG probe. (B) Representative confocal microscopy images of the C2C12 cells loaded with a 100 µM 2-NBDG probe for 30 minutes and treated with palmitate (0.75 mM and 16 hours) ± SAC (100 µM and 30 minutes) and ± insulin (100 nM and 30 minutes). Scale bars: 30 µm. Confocal microscopy images (60×) are presented in pseudocolor (LUT = fire) to better show the fluorescence intensity variations. (C) Bar graph summarizing the effect of PA and reversion with SAC in insulin-resistant cells in the same experimental condition described in (B). No significant differences were observed between insulin and SAC stimulation. Fluorescence was evaluated using a microplate reader ($465_{Ex}/540_{Em}$ nm). Data in percentage referred to the control condition of $n = 4$ independent experiments are represented as mean ± SEM. ***$p < 0.001$ (ANOVA followed by the Bonferroni *post hoc* test). The values are as follows: (C) Ctrl: 100.00 ± 6.72; Ins: 155.79 ± 5.40; SAC: 157.69 ± 5.81; PA: 99.17 ± 4.52; PA + Ins: 101.06 ± 7.15; and PA + SAC: 140.15 ± 5.53.

thus supporting the idea of the involvement of the insulin receptor in mediating the effect of SAC on glucose metabolism. The results of differential scanning calorimetry (DSC) experiments highlight a clear interaction between SAC and the insulin receptor kinase domain (INSR), evidenced by a leftward shift in the thermogram. This indicates a reduction in thermal stability upon ligand binding. While ligand interactions often lead to increased protein stability, as typically observed for inhibitors, this is not always the case for positive modulators or allosteric activators, as suggested in the case of SAC.[33] Molecular docking simulations further support the atypical nature of the interaction. SAC does not appear to bind near the canonical ATP-binding site, typically targeted by competitive inhibitors, but instead localizes to a distinct regulatory region near the binding interface of GRB14. The best-scoring docking poses (energy ≈ 4.9 kcal mol^{-1}) consistently involved residues such as R1039, M1153, and notably pY1163, suggesting a binding mode that is structurally peripheral and likely allosteric in nature. This site lies outside the catalytic cleft, yet within a functionally important region involved in the regulation of activation. The binding mode of SAC appears to be transient and only partially buried, as hydrogen bonding and contact residues are predominantly located in lateral domains (Fig. 3E and F), not in the deeply buried catalytic

core. This supports the hypothesis that SAC does not stabilize the receptor structure, but rather induces flexibility or disrupts native interactions, potentially leading to local unfolding or rearrangement. This correlates with the observed decrease in T_m (Fig. 4), consistent with ligand-induced destabilization. Functionally, SAC may compete with the endogenous inhibitory adaptor GRB14, which binds to the same regulatory surface. GRB14 inhibits INSR by acting as a pseudosubstrate and stabilizing its inactive conformation. SAC could partially displace GRB14, thereby alleviating its inhibitory effect without fully replacing it. This partial displacement may be sufficient to restore a residual basal activity of the kinase, enabling phosphorylation of downstream effectors, as observed in cell-based assays. In addition, PTP1B, the phosphatase responsible for dephosphorylating Y1163 and inactivating the receptor, may also be affected. If SAC binds in a way that alters the positioning of GRB14 without fully removing it, the access of PTP1B to the activation loop could be sterically hindered. Thus, SAC may act as a dual modulator, both relieving GRB14-mediated inhibition and preventing phosphatase-driven inactivation. Taken together, these findings support a model in which SAC exerts positive allosteric modulation of INSR activity, not by classical activation, but by interfering with negative regulatory mechanisms. This may explain the observed insulin mimetic activity of SAC *in vitro* and support further exploration of SAC-like compounds as non-competitive modulators of insulin signaling. These molecular observations align well with the cellular effects previously reported for SAC, reinforcing its potential as a pharmacological tool or lead compound for modulating insulin receptor signaling.

The second goal of this work was to evaluate the potential role of SAC in preventing or reversing insulin resistance in a palmitate-induced insulin-resistant C2C12 model.

The skeletal muscle is the major site for the disposal of ingested glucose in healthy individuals. In insulin-resistant states, these insulin-stimulated glucose disposals are markedly impaired. Although the mechanisms responsible for the onset of insulin resistance are not yet fully elucidated, the role of increased free fatty acids (FFAs) is now well established.[30] According to Yudhani *et al.*,[31] to induce insulin resistance in our cellular model, C2C12 cells were treated with palmitic acid (0.75 mM) for 16 hours. Before proceeding with the induction of insulin resistance, the effects of 24-hour treatment with PA on C2C12 cytotoxicity and intracellular ROS production were evaluated. Our results manifested that PA did not affect cellular viability at any tested concentration (Fig. 5A). Moreover, 0.75 mM PA did not enhance ROS production in comparison to the positive control menadione (Fig. 5B). Therefore, to evaluate the effect of SAC on the insulin-resistant state, cells were treated with 0.75 mM PA for 16 h. As shown in Fig. 6 and 7, C2C12 cells were considered insulin resistant after 16 hours of treatment with PA, since they no longer responded to acute insulin stimulation in terms of glucose uptake. However, the co-treatment of SAC for 16 hours with PA (Fig. 6) restored the ability of C2C12 cells to respond to insulin, demonstrating an effect of SAC in preventing insulin resistance. Moreover, the addition of 100 μM SAC during the final 30 minutes of PA treatment was sufficient to rescue the effect of palmitic acid, supporting an effect of SAC also in reversing insulin resistance (Fig. 7). In our hypothesis, this effect could be mediated by the ability of SAC in preserving the insulin receptor activity and in reverting its impairment, rather than in restoring PA-induced lipotoxicity, as in our model, PA was not cytotoxic and did not affect ROS production. This hypothesis is supported by the study of Luo *et al.*, in which S-Allylmercaptocysteine restored the downstream IRS-1/AKT/GSK3b signaling in ethanol-treated hepatocytes through direct binding with the insulin receptor.[20] Despite our findings, there are some limitations in the present study. First of all, the study was conducted only *in vitro*, using a cellular model of normal and insulin-resistant skeletal myotubes. A study in animal models, and subsequently in humans, will be necessary to confirm our results and assess the effects of SAC. Moreover, while the present work focuses on the molecular mechanisms underlying the insulin-mimetic effects of SAC, we acknowledge that additional confirmatory experiments aimed at the measurement of binding affinity (isothermal titration calorimetry) and kinetics (surface plasmon resonance) are required to further validate the binding between SAC and the insulin receptor. Therefore, future studies will be specifically dedicated to the full biophysical characterization of the ligand–receptor complex.

Conclusions

In conclusion, our study highlights the beneficial role of SAC obtained from black garlic and black garlic extracts for dietary supplements. SAC works primarily through its antioxidant properties and through binding to the insulin receptor, resulting in the regulation of glucose metabolism in C2C12 skeletal muscle cells. In particular, SAC, like insulin, promotes *de novo* protein synthesis, GLUT4 translocation from the cytoplasm to the plasma membrane, and thus glucose uptake. Furthermore, SAC can prevent and reverse the condition of insulin resistance in C2C12 cells. Taken together with our previous findings about the protective role of SAC on endothelial health,[17] our results support and reinforce the potential use of SAC as a useful bioactive compound for the prevention and the onset of metabolic syndrome, a pathologic condition characterized by insulin resistance, dyslipidemia and hypertension, nowadays considered as a "Global epidemic". Moreover, the high oral bioavailability and remarkable plasma stability of SAC, consistently reported across animal and human studies[34] together with its excellent safety profile, showing no adverse effects below 250 mg kg^{-1} and only mild toxicity at supraphysiological doses above 500 mg kg^{-1},[35] further strengthen its suitability as a nutritionally relevant bioactive compound. These features support its potential inclusion in nutraceutical strategies aimed at preventing or mitigating MetS and related metabolic disorders.

Author contributions

Conceptualization: M. P. G.; F. G.; and S. A. Data curation: F. G. and S. A. Formal analysis: F. G.; S. A; L. C.; G. C.; and G. C. Funding acquisition: M. P. G. Investigation: F. G.; S. A.; A. O.; L. C.; G. C.; and G. C. Methodology F. G.; S. A.; L. C.; G. C.; G. C; and M. P. G. Project administration M. P. G. and S. A. Resources: M. P. G. and G. G. Software: F. G.; S. A.; L. C.; G. C.; and G. C. Supervision: M. P. G. and G. G. Validation: F. G.; S. A.; G. Q.; A. O.; L. C.; G. C.; G. C; and M. P. G. Visualization: F. G.; S. A.; G. Q.; A. O.; L. C.; G. C.; G. C; and M. P. G. Writing – original draft: F. G.; S. A.; L. C.; G. C.; G. C; and M. P. G. Writing – review and editing: F. G.; S. A.; G. Q.; A. O.; G. G.; L. C.; G. C.; G. C; and M. P. G.

Conflicts of interest

L. C. is employed by Abel Nutraceuticals S.r.l.; L. C. is a student of the Ph.D. Program in Pharmaceutical and Biomolecular Sciences of the University of Turin (XXXIX cycle) and in apprenticeship at Abel Nutraceuticals S.r.l. The remaining authors declare that the research was conducted in the absence of any commercial or financial relationships that could be construed as a potential conflict of interest.

Data availability

All the experimental data presented in this Original Research Article are stored in the institutional cloud of the University of Torino and are available upon request from the corresponding author (mariapia.gallo@unito.it).

Acknowledgements

This work was supported by the local funding of the University of Turin (Maria Pia Gallo). We thank Biosfered S.r.l. for kindly providing S-allyl cysteine and the protein kinase domain (Leu1067–Gly1296) of the Mouse Insulin Receptor.

References

1 T. K. C. Le, X. D. Dao, D. V. Nguyen, D. H. Luu, T. M. H. Bui, T. H. Le, H. T. Nguyen, T. N. Le, T. Hosaka and T. T. T. Nguyen, Insulin signaling and its application, *Front. Endocrinol.*, 2023, **14**, 1226655.

2 M. Li, X. Chi, Y. Wang, S. Setrerrahmane, W. Xie and H. Xu, Trends in insulin resistance: insights into mechanisms and therapeutic strategy, *Signal Transduction Targeted Ther.*, 2022, **7**, 216.

3 M. A. Abdul-Ghani and R. A. DeFronzo, Pathogenesis of insulin resistance in skeletal muscle, *J. Biomed. Biotechnol.*, 2010, **2010**, 476279.

4 S.-H. Lee, S.-Y. Park and C. S. Choi, Insulin Resistance: From Mechanisms to Therapeutic Strategies, *Diabetes Metab. J.*, 2022, **46**, 15–37.

5 C. E. Kosmas, M. D. Bousvarou, C. E. Kostara, E. J. Papakonstantinou, E. Salamou and E. Guzman, Insulin resistance and cardiovascular disease, *J. Int. Med. Res.*, 2023, **51**, 3000605231164548.

6 M. Marušić, M. Paić, M. Knobloch and A. M. Liberati Pršo, NAFLD, Insulin Resistance, and Diabetes Mellitus Type 2, *Can. J. Gastroenterol. Hepatol.*, 2021, **2021**, 6613827.

7 S. C. da Silva Rosa, N. Nayak, A. M. Caymo and J. W. Gordon, Mechanisms of muscle insulin resistance and the cross-talk with liver and adipose tissue, *Physiol. Rep.*, 2020, **8**, e14607.

8 M. Mirabelli, E. Chiefari, B. Arcidiacono, D. M. Corigliano, F. S. Brunetti, V. Maggisano, D. Russo, D. P. Foti and A. Brunetti, Mediterranean Diet Nutrients to Turn the Tide against Insulin Resistance and Related Diseases, *Nutrients*, 2020, **12**, 1066.

9 C. K. Roberts, A. L. Hevener and R. J. Barnard, Metabolic syndrome and insulin resistance: underlying causes and modification by exercise training, *Compr. Physiol.*, 2013, **3**, 1–58.

10 B. Yudhistira, F. Punthi, J.-A. Lin, A. S. Sulaimana, C.-K. Chang and C.-W. Hsieh, S-Allyl cysteine in garlic (Allium sativum): Formation, biofunction, and resistance to food processing for value-added product development, *Compr. Rev. Food Sci. Food Saf.*, 2022, **21**, 2665–2687.

11 T. Ahmed and C.-K. Wang, Black Garlic and Its Bioactive Compounds on Human Health Diseases: A Review, *Molecules*, 2021, **26**, 5028.

12 A. L. Colín-González, S. F. Ali, I. Túnez and A. Santamaría, On the antioxidant, neuroprotective and anti-inflammatory properties of S-allyl cysteine: An update, *Neurochem. Int.*, 2015, **89**, 83–91.

13 A. Bentke-Imiolek, D. Szlęzak, M. Zarzycka, M. Wróbel and P. Bronowicka-Adamska, S-Allyl-L-Cysteine Affects Cell Proliferation and Expression of H_2S-Synthetizing Enzymes in MCF-7 and MDA-MB-231 Adenocarcinoma Cell Lines, *Biomolecules*, 2024, **14**, 188.

14 P. Chen, C. Chen, M. Hu, R. Cui, F. Liu, H. Yu and Y. Ren, S-allyl-L-cysteine protects hepatocytes from indomethacin-induced apoptosis by attenuating endoplasmic reticulum stress, *FEBS Open Bio*, 2020, **10**, 1900–1911.

15 G. Luo, Z. Wu, Q. Fan, C. Zhang, J. Lin, H. Li, J. Zhao, H. Huo, X. Qi, G. Wu, M. Chen, J. Yu, L. Zheng and M. Luo, S-Allyl-Cysteine Ameliorates Cirrhotic Portal Hypertension by Enhancing Lymphangiogenesis via a VEGF-C-Independent Manner, *Liver Int.*, 2025, **45**, e70024.

16 Y. Kosuge, Neuroprotective mechanisms of S-allyl-L-cysteine in neurological disease, *Exp. Ther. Med.*, 2020, **19**, 1565–1569.

17 F. Geddo, G. Querio, A. Asteggiano, S. Antoniotti, A. Porcu, A. Occhipinti, C. Medana and M. P. Gallo, Improving endothelial health with food-derived H_2 S donors: an *in vitro* study with *S* -allyl cysteine and with a black-garlic extract

enriched in sulfur-containing compounds, *Food Funct.*, 2023, **14**, 4163–4172.
18 G. Saravanan and P. Ponmurugan, Beneficial Effect of S-allylcysteine (SAC) on Blood Glucose and Pancreatic Antioxidant System in Streptozotocin Diabetic Rats, *Plant Foods Hum. Nutr.*, 2010, **65**, 374–378.
19 G. Saravanan and P. Ponmurugan, Ameliorative potential of S-allyl cysteine on oxidative stress in STZ induced diabetic rats, *Chem.-Biol. Interact.*, 2011, **189**, 100–106.
20 P. Luo, M. Zheng, R. Zhang, H. Zhang, Y. Liu, W. Li, X. Sun, Q. Yu, G. L. Tipoe and J. Xiao, S-Allylmercaptocysteine improves alcoholic liver disease partly through a direct modulation of insulin receptor signaling, *Acta Pharm. Sin. B*, 2021, **11**, 668–679.
21 F. Geddo, G. Querio, A. Asteggiano, S. Antoniotti, A. Porcu, A. Occhipinti, C. Medana and M. P. Gallo, Improving endothelial health with food-derived H_2 S donors: an *in vitro* study with *S* -allyl cysteine and with a black-garlic extract enriched in sulfur-containing compounds, *Food Funct.*, 2023, **14**, 4163–4172.
22 H. Cheropkina, G. Catucci, A. Marucco, I. Fenoglio, G. Gilardi and S. J. Sadeghi, Human flavin-containing monooxygenase 1 and its long-sought hydroperoxyflavin intermediate, *Biochem. Pharmacol.*, 2021, **193**, 114763.
23 A. Schiavon, L. Saba, G. Catucci, J. Petiti, S. Puglisi, C. Borin, G. Reimondo, G. Gilardi, C. Giachino, M. Terzolo and M. Lo Iacono, Albumin/Mitotane Interaction Affects Drug Activity in Adrenocortical Carcinoma Cells: Smoke and Mirrors on Mitotane Effect with Possible Implications for Patients' Management, *Int. J. Mol. Sci.*, 2023, **24**, 16701.
24 R. S. Depetris, J. Hu, I. Gimpelevich, L. J. Holt, R. J. Daly and S. R. Hubbard, Structural Basis for Inhibition of the Insulin Receptor by the Adaptor Protein Grb14, *Mol. Cell*, 2005, **20**, 325–333.
25 O. Trott and A. J. Olson, AutoDock Vina: Improving the speed and accuracy of docking with a new scoring function, efficient optimization, and multithreading, *J. Comput. Chem.*, 2010, **31**, 455–461.
26 F. Favretto, E. Jiménez-Faraco, G. Catucci, A. Di Matteo, C. Travaglini-Allocatelli, S. J. Sadeghi, P. Dominici, J. A. Hermoso and A. Astegno, Evaluating the potential of non–immunosuppressive cyclosporin analogs for targeting *Toxoplasma gondii* cyclophilin: Insights from structural studies, *Protein Sci.*, 2024, **33**, e5157.
27 Y. Sun, Z. Yang, F. Ren and B. Fang, FGF19 alleviates palmitate-induced atrophy in C2C12 cells by inhibiting mitochondrial overload and insulin resistance, *Int. J. Biol. Macromol.*, 2020, **158**, 401–407.
28 S. Penislusshiyan, L. Chitra, I. Ancy, P. Kumaradhas and T. Palvannan, Novel antioxidant astaxanthin-s-allyl cysteine biconjugate diminished oxidative stress and mitochondrial dysfunction to triumph diabetes in rat model, *Life Sci.*, 2020, **245**, 117367.
29 P. Sakayanathan, C. Loganathan and P. Thayumanavan, Astaxanthin–S–Allyl Cysteine Ester Protects Pancreatic β–Cell From Glucolipotoxicity by Suppressing Oxidative Stress, Endoplasmic Reticulum Stress and mTOR Pathway Dysregulation, *J. Biochem. Mol. Toxicol.*, 2024, **38**, e70058.
30 M. A. Abdul-Ghani and R. A. DeFronzo, Pathogenesis of Insulin Resistance in Skeletal Muscle, *J. Biomed. Biotechnol.*, 2010, **2010**, 1–19.
31 R. D. Yudhani, Y. Sari, D. A. A. Nugrahaningsih, E. N. Sholikhah, M. Rochmanti, A. K. R. Purba, H. Khotimah, D. Nugrahenny and M. Mustofa, In Vitro Insulin Resistance Model: A Recent Update, *J. Obes.*, 2023, **2023**, 1–13.
32 P. Gupta, V. Dutt, N. Kaur, P. Kalra, S. Gupta, A. Dua, R. Dabur, V. Saini and A. Mittal, S-allyl cysteine: A potential compound against skeletal muscle atrophy, *Biochim. Biophys. Acta, Gen. Subj.*, 2020, **1864**, 129676.
33 S. K. Bardal, *Applied pharmacology*, Elsevier/Saunders, St. Louis, Mo, 2011.
34 M. Nakamoto, K. Kunimura and M. Ohtani, Pharmacokinetics of sulfur-containing compounds in aged garlic extract: S-Allylcysteine, S-1-propenylcysteine, S-methylcysteine, S-allylmercaptocysteine and others (Review), *Exp. Ther. Med.*, 2025, **29**, 102.
35 Y. Kodera, A. Suzuki, O. Imada, S. Kasuga, I. Sumioka, A. Kanezawa, N. Taru, M. Fujikawa, S. Nagae, K. Masamoto, K. Maeshige and K. Ono, Physical, Chemical, and Biological Properties of S-Allylcysteine, an Amino Acid Derived from Garlic, *J. Agric. Food Chem.*, 2002, **50**, 622–632.

